Spectrochimica Acta Part A: Molecular and Biomolecular Spectroscopy 225 (2020) 117524

Contents lists available at ScienceDirect

Spectrochimica Acta Part A: Molecular and Biomolecular Spectroscopy

journal homepage: www.elsevier.com/locate/saa

From aerospace to screen: Multifunctional poly(benzoxazine)s based on different triarylamines for electrochromic, explosive detection and resistance memory devices

Yan Wang [a], Haiying Niu [b], Qingyi Lu [a], Wei Zhang [a], Xin Qiao [a], Haijun Niu [a,*], Yanhong Zhang [a,*], Wen Wang [c,*]

[a] *Key Laboratory of Functional Inorganic Material Chemistry, Ministry of Education, Department of Macromolecular Science and Engineering, School of Chemical, Chemical Engineering and Materials, Heilongjiang University, Harbin 150086, PR China*

[b] *Daxinganlingshiyan Middle School, Heilongjiang Province 16500, PR China*

[c] *School of Materials Science and Engineering, Harbin Institute of Technology, Harbin 150080, PR China*

ARTICLE INFO

Article history:
Received 10 August 2019
Received in revised form 7 September 2019
Accepted 8 September 2019
Available online 10 September 2019

Keywords:
Benzoxazine
Triarylamine
Explosive detection
Fluorescence
Resistance memory

ABSTRACT

Four kinds of main-chain benzoxazine polymers (PBZ) containing triarylamine (TAA) units were synthesized by Mannich reaction and characterized by ^{1}H nuclear magnetic resonance (NMR), Fourier transform infrared (FT-IR) techniques, etc. Thermal, optical, photophysical and electrochemical properties were studied. The 50% of char residue is left in N_2 at 800 °C. The polymers are soluble in common organic solvents and easily spin-coated onto indium tin oxide (ITO) coated glass substrates. All the polymers have voltage window ranging from 0 to 1.8 V, and the colors change from yellowish to dark red when voltage is applied. Meanwhile, device assembled from polymer exhibit significant color changes. Furthermore, the polymers also have promising potential application in explosive detection and resistance memory devices.

1. Introduction

Electrochromic (EC) materials have caught the attention by scientists for many years [1–4]. The phenomenon that the reversible color changes provided that adequate potential is applied on the EC material is defined as electrochromism [5–8]. EC materials have found an increasingly wide utilization in many fields, such as, displays devices, electronic paper and so on [9–12]. EC materials can be classified into two big families including inorganic EC materials such as tungsten trioxide (WO_3), and organic or polymer EC materials such as phthalocyanines, polythiophene (PTh), polyaniline (PAn) and so on [13–15]. In recent years, EC materials are becoming more and more intelligent, such as, Wang's group showed the ambient-driven actuator with a commercial acid ionomer film which can safely contact skin. Jia's team reported that the copolymer EC film with flexible and stretchable performances acted like natural chameleon skin. These examples reflect electrochromism has a broader exploration prospect. The triarylamine (TAA) derivatives have been focused on for many years due to excellent donor and charge transport properties in Organic Light Emitting Diode (OLED), Organic Photovoltaic Solar Cell (OPV) and EC. Many groups synthesized a great deal of different kinds of polymers containing TAA and researched their electro-optical properties deeply [16].

As for PBZ, due to a wide range of interesting features, such as near-zero shrinkage [17], excellent heat resisting property, low surface free energy [18], agile molecular design, it plays an important role in the aeronautical astronautical technologies [19,20], refractories, insulating materials, medicine and chemical industry. BZ is a six membered heterocyclic compound containing N and O, which is prepared via Mannich reaction of phenol, amines and paraformaldehyde. PBZ can be prepared by curing precursors successfully. In view of the advantages and the wider application prospects of PBZ, many scientists have made many attempts to combine BZ with other multifunctional materials. Liou's group has prepared flexible PBZ films containing TAA in 2014 [21], followed by Ishida's group reported on the successful polymerization of fused-ring BZs and naphthoxazines in 2017 [22]. And recently PBZs containing organic/inorganic hybrid materials incorporating silicon-based species and carbon-based species have been explored [23].

In order to combine inherent thermal advantages of BZ with electrooptical properties, and effectively modulate the electrooptical properties, we designed and synthetized four kinds of main-chain BZs polymers with good film-forming capability from selected TAA-based diamines and naphthalene-based diamines. The relationship of structure-property is studied, and the optical band can be tuned finely by changing the structure of TAA. These polymers also have good EC behavior with high optical transmittance change.

---

* Corresponding authors.
E-mail addresses: haijunniu@hotmail.com (H. Niu), zhangyanhong@hlju.edu.cn (Y. Zhang), wangwen@hit.edu.cn (W. Wang).

https://doi.org/10.1016/j.saa.2019.117524
1386-1425/

2. Experimental section

2.1. Methods, materials

A detailed description of the materials, methods are shown in the support information.

2.2. Synthesis of monomers and polymers

The synthetic routes of the monomers (M1, M2, M3, and M4) and polymers (P1, P2, P3, and P4) are shown in Scheme 1, in which monomers were synthesized in modified way according to our reported articles [24,25].

The synthetic process of P1 is illustrated as an example. M1 (0.50 g, 1.13 mmol), 9,9-bis(4-hydroxyphenyl)fluorene (0.40 g, 1.13 mmol) was charged into a three-neck round-bottomed flask under nitrogen atmosphere, then 7.2 mL toluene-ethanol mixture (Vol:Vol = 1:2) was added and the mixture was stirred at room temperature. When it almost changed into homogeneous solution, paraformaldehyde was added (0.14 g, 4.52 mmol) into the flask, then the mixture was slowly heated to 80 °C for 48 h. After cooled to the room temperature, it was poured into methanol slowly. The final product was filtered and purified by Soxhlet extractor with methanol. Yield: 71.2%, yellow powder solid, IR (KBr, cm^{-1}): 938 (oxazine ring), 1280 (CH_2 wag). ^1H NMR (400 MHz, DMSO d_6, δ, ppm): 5.3–4.5 (oxazine ring), 7.8–6.5 (aromatic ring of benzene).

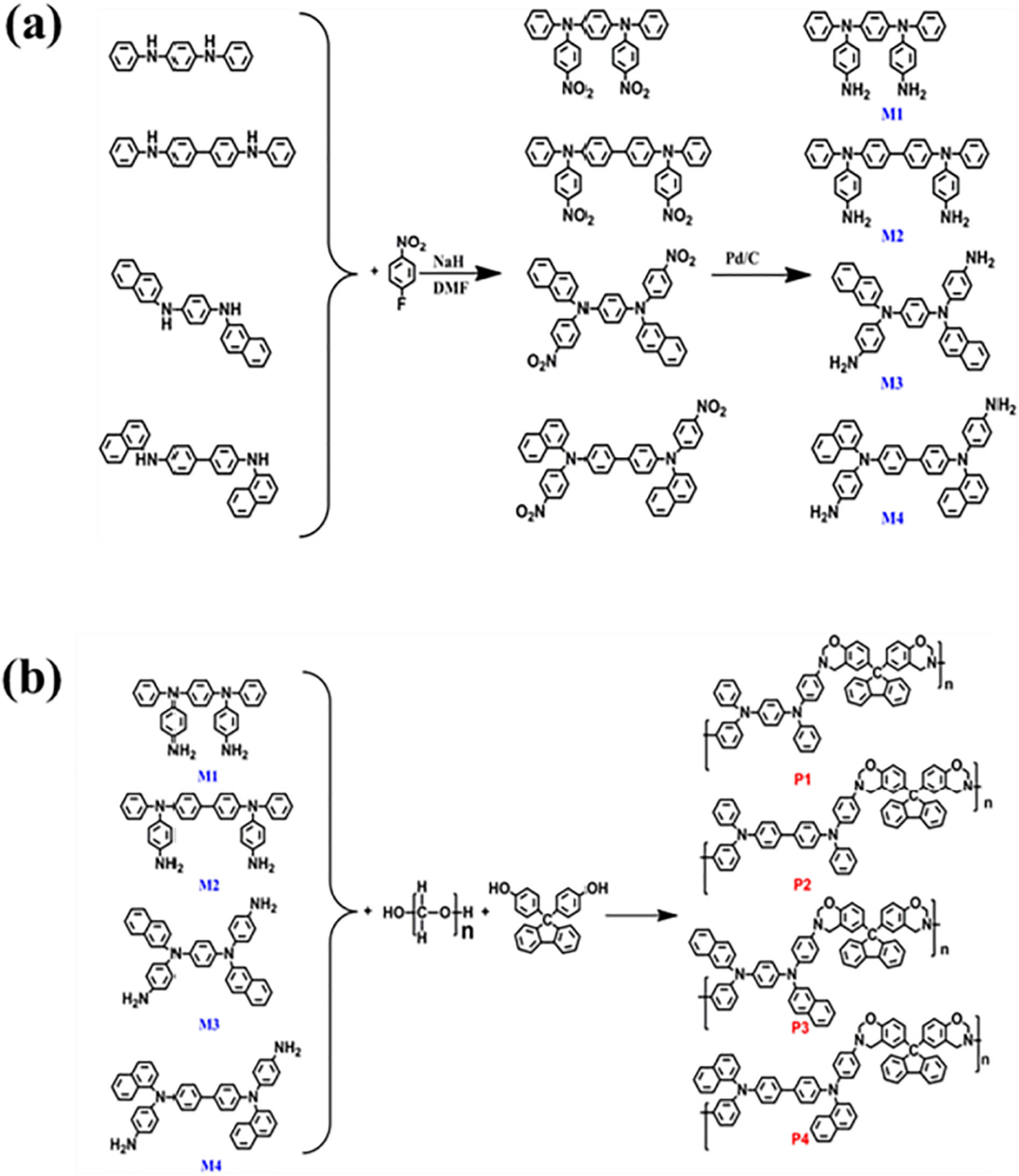

Scheme 1. Synthetic routes of the monomers M1–M4 (a) and polymers P1–P4 (b).

P2: Yield: 73.5%. A yellow particle, IR (KBr, cm^{-1}): 934 (oxazine ring), 1269 (CH_2 wag). ^1H NMR (400 MHz, DMSO d_6, δ, ppm): 5.5–4.5 (oxazine ring), 8.1–6.7 (aromatic ring of benzene).

P3: Yield: 70.5%. A light yellow particle, IR (KBr, cm^{-1}): 940 (oxazine ring), 1342 (CH_2 wag). ^1H NMR (400 MHz, DMSO d_6, δ, ppm): 5.5–4.5 (oxazine ring), 8.0–6.4 (aromatic ring of benzene).

P4: Yield: 71.5%. A dark yellow particle, IR (KBr, cm^{-1}): 940 (oxazine ring), 1386 (CH_2 wag). ^1H NMR (400 MHz, DMSO d_6, δ, ppm): 5.5–4.5 (oxazine ring), 8.1–6.5 (aromatic ring of benzene).

2.3. Preparation of the polymer films and WO_3 film

Firstly, 0.1 g polymer sample was dissolved into *N*-methyl-2-pyrrolidinone (NMP). Then, the homogeneous solution of the polymer sample was dripped onto the 1 cm × 5 cm of ITO, followed by being uniformly distributed through a spin coater at a speed of 500 rpm. Finally, the film was dried in vacuum at 100 °C for 12 h. To give a deep explanation for the test, the polymer films thicknesses were tested by an interference microscope, which of P1, P2, P3 and P4 are 95 nm, 115 nm, 100 nm and 120 nm, respectively. To improve the contrast ratio, the WO_3 electrode was introduced in the EC device. By a low-temperature sol-gel process the ECD WO_3 film on ITO was obtained and the specific preparation process was described in detail in elsewhere [26,27]. Here, WO_3 film and the polymer active film were coated on two pieces of ITO with the same area worked as cathode and the anode (thicknesses are 93 nm, 98 nm, respectively.).

3. Results and discussion

3.1. Characterization of monomers and polymers

The four diamine monomers were obtained by previous work of our group. NMR FT-IR spectrometers were used to confirm the structures of monomers and polymers.

Take P4 as an example, the peaks appear at the range of 4.5–5.5 ppm in ^1H NMR spectrum which confirms the presence of oxazine ring, and the peaks within the scope of 6.48–8.13 ppm are representing aromatic hydrogens. The peaks at about 940 cm^{-1} in IR spectra (Fig. 1) are ascribed to oxazine vibration. From the results of IR and NMR data confirm that the expected structure is obtained successfully. Figs. S1, S2, and S3 also confirm the proposed structures of P1, P2, and P3.

3.2. Thermal properties and solubility

The thermal stability plays a positive role in the application of the material. All polymers show similar degradation profiles (shown in Fig. 2). The 10% weight loss of these polymers decomposition temperatures (T_d) in N_2 is in the range of 410–490 °C. Also, these polymers still remain high char yields about 56%–67% at 800 °C. Moreover, the T_d of weight loss at 5%, 10% and 20% are summarized in Table 1. As seen in the Table 1, the order of the four polymers char yields is: P4 > P3 > P2 > P1. The most likely reason is that the naphthalene rings in P3 and P4 makes it harder for the polymers to decompose during being heated in high temperature region. At the same time, the more the polymers have benzene rings in the main chain, the higher they show thermal properties.

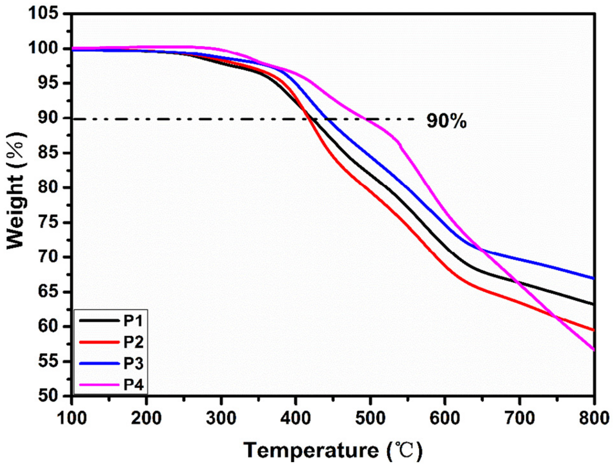

Fig. 2. Thermogravimetric (TGA) curves of four polymers.

The better solubility enlarges the application area of these polymers. 10 mg of polymer was dissolved in various solvents (methanol, NMP, dimethylsulfoxide (DMSO), tetrahydrofuran (THF), dichloromethane and the results are summarized in Table S1. As it is seen from the table, P3 and P4 are less soluble as compared to P1 and P2 which might be due to the presence of more benzene rings facilitating the aggregation of P3 and P4. Meanwhile the molecular weights of these polymers including number-average ($\overline{M}_n$), weight-average ($\overline{M}_w$), and polydispersity index (PDI) were evaluated through gel permeation chromatography (GPC) technique. The specific data are shown in Table 1 which indicates these polymers have different PDI, lower degree of polymerization (DP) and medium molecular weights. A high molecular weight can be obtained by polymerization according to the synthesis route, however in the GPC test; some part of the polymer precipitated during the test so that GPC results came from those with low molecular weight which could be soluble fractions.

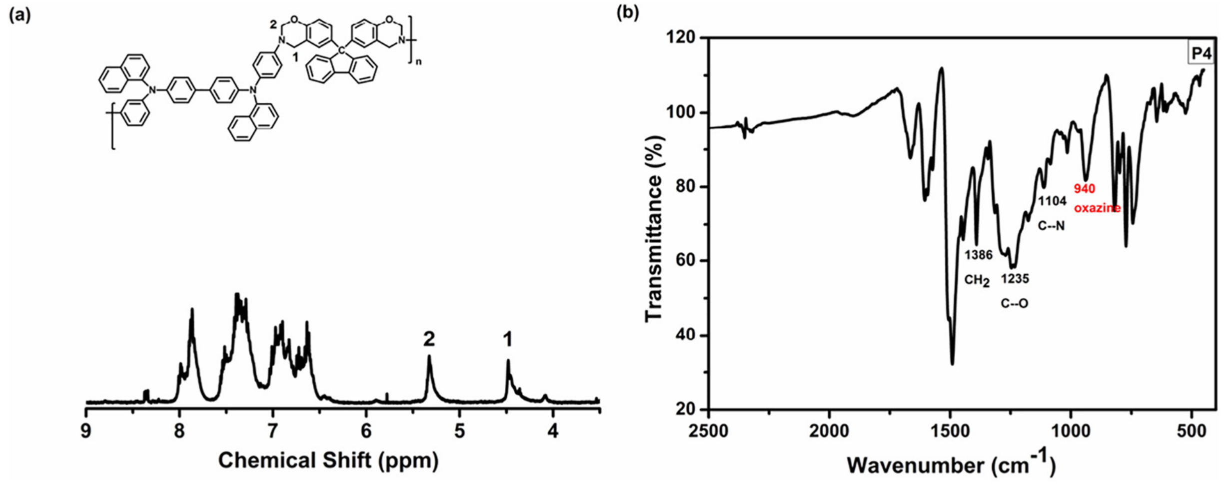

Fig. 1. The ^1H NMR spectrum (a) and FT-IR spectrum (b) of P4.

Table 1
Thermal properties and molecular weights of the polymers.

Polymer code	T^{a}5% °C	T^{a}20% °C	Chair yield[b] (wt%)	$\overline{M}_w$[c] (Da)	$\overline{M}_n$[c] (Da)	PDI	DP[d]
P1	419	576	56	7.0×10^3	4.2×10^3	1.67	8.3
P2	380	493	59	7.6×10^3	5.0×10^3	1.52	8.2
P3	372	521	63	8.2×10^3	5.2×10^3	1.58	8.7
P4	400	550	67	8.6×10^3	5.6×10^3	1.53	8.4

[a] The T_d of polymers weight losses at 5% and 20% in nitrogen.
[b] Measured at 800 °C in nitrogen.
[c] Dispersity: $\overline{M}_w/\overline{M}_n$.
[d] Degree of polymerization.

Table 2
Optical properties of the polymers.

Polymer		In solution[a] λ (nm)		As film λ (nm)	
Code	Abs_{max}	PL_{max}	φ_{PL} (%)[b]	Abs_{max}	Abs_{onset}
P1	353	486	2.4	367	501
P2	345	475	46	394	514
P3	343	530	2.2	371	406
P4	351	520	14	398	492

[a] 1×10^{-4} mol/L NMP solution for measured.
[b] Quinine sulfate used as reference standard ($\varphi_{PL} = 54.6\%$) for measured.

3.3. Optical properties

The UV–vis and photoluminescence (PL) data are summarized in Table 2. P2 and P4 exhibit strong UV–vis absorption at about 350 nm in NMP solution which can be attributed to the π–π* transition of the TAA seen from the Fig. 3(a) [28,29]. The large Stokes shift (133, 130, 187 and 169 nm for P1, P2, P3 and P4, respectively) from the Table 2, we ascribe the Stokes shift to a certain energy loss in process of emission compared to the process of excitation. The Stokes shift mainly depends on the change of the molecular equilibrium configurations between the ground state and excited state. During the transition, the greater is the difference in molecular equilibrium configuration from ground to exited

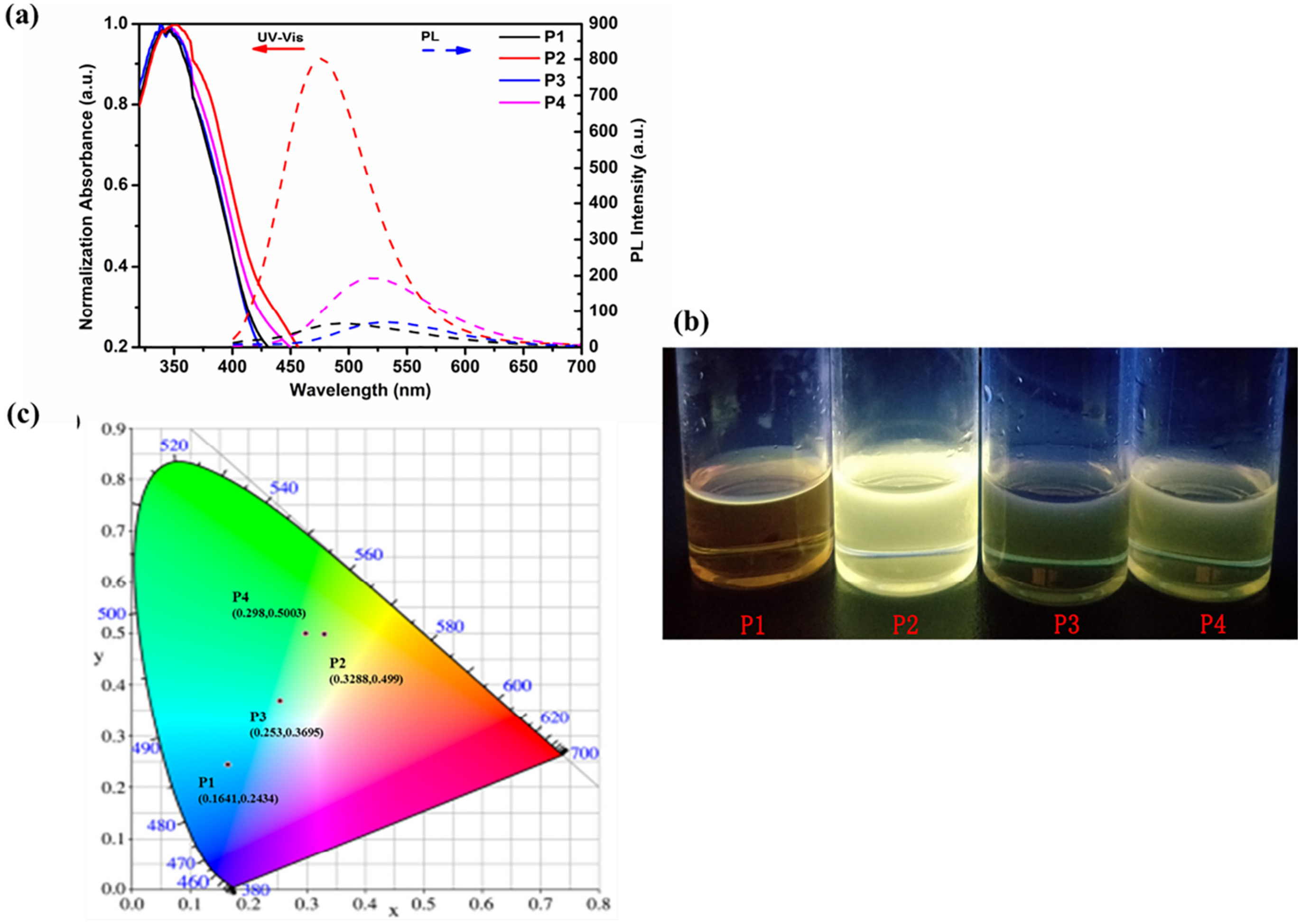

Fig. 3. UV–vis and PL spectra of P1 to P4 at room temperature in NMP solution (1×10^{-5} mol/L) (a). Photographs taken under 365 nm UV light illumination (b) and the CIE 1931 (x,y) chromaticity diagram (c) of the these polymers. (For interpretation of the references to color in this figure, the reader is referred to the web version of this article.)

state, the greater does the emission energy lose due to the energy consuming of molecular vibrational, and the larger is the Stokes shift. As a result, the larger Stokes shift of P3 and P4 compared with P1 and P2 may come from the large energy loss in the emission of conjugated structures. According to the following formula (1), it can be seen that there is a complex relationship between Stokes shift and μ, solvent. The electron transition causes the redistribution of the electron cloud, so the dipole moment of the ground state and excited state of molecules are generally different, and the influence of solvent polarity molecules on the ground state and excited state of molecules is different. We may speculate that the Stokes shifts of P3 and P4 are larger due to the larger dipole moment change between the ground state and excited state compared to P1 and P2.

$$\tilde{V}_{abs}-\tilde{V}_{F}\approx\frac{2}{4\pi\varepsilon_{0}hcr_{w}^{3}}(\mu_{E}-\mu_{G})^{2}\Delta f+Const \tag{1}$$

The optical properties of the polymer were mainly studied through the analysis of UV–vis spectra and PL spectra. The φ_{PL}s of the four polymers in NMP solution were calculated by the following formula (2). In the formula (2) φ_{unk}, I_{unk}, A_{unk}, η_{unk}, φ_{std}, I_{std}, A_{std} and η_{std} are PL quantum efficiency, PL integral area excited at the excitation wavelength, absorbance intensity and corresponding refractive index of solution for the sample (noted as unk) and reference standard (noted as std), respectively. The quinine sulfate in thin sulfuric acid was used as std (φ_{PL} = 54.6%) for measured. From the Table 2 which P2 and P4 have the stronger PL peaks than these of P1 and P3 with the φ_{PL} of P1, P2, P3 and P4 being 2.4%, 46%, 2.2% and 14%, respectively. As Fig. 3(b) and (c) indicating that P2 and P4 emit stronger bright yellow PL and dark yellow PL, respectively. Meanwhile, P1 and P3 exhibit weak yellow-blue PL and weak yellow-green PL, respectively. However, the λ_{max} of P2 and P4 exhibit nearly 20 nm red shift compared with the P1 and P3. The above results can be explained by the rigid and conjugated structures of P2 and P4 are more planar and longer than these of P1 and P3 [30,31]. At the same time, it can be seen from Table 1 that the solid films of P2 and P4 generate obvious red shift relative to the dilute solution in the absorption spectra, which may be caused by the strong intermolecular interaction in the solid that makes the biphenyl conformation tend to be planar and increases the conjugated length of the polymers.

$$\varphi_{unk}=\varphi_{std}\left(\frac{I_{unk}}{I_{std}}\right)\left(\frac{A_{std}}{A_{unk}}\right)\left(\frac{\eta_{unk}}{\eta_{std}}\right)^{2} \tag{2}$$

3.4. Electrochemical properties with quantum chemistry calculation

The electrochemical data can be used for calculating energy level and energy gap. The detailed data of the CV testing are summarized in the Table 3. The $E_{1/2}$ values of P1 are 0.69 V (E_{onset} = 0.52 V) and 1.00 V. $E_{1/2}$ values of P3 are 0.70 V (E_{onset} = 0.35 V) and 0.96 V. The $E_{1/2}$ values of P2 and P4 are 0.94 V (E_{onset} = 0.73 V), and 1.00 V (E_{onset} = 0.53 V), respectively. It is generally believed that the conjugated structure will have the narrower E_g because combination of the raised HOMO level and the decreased LUMO. The half wave potentials and onset potentials for the polymers are mainly related to the HOMO, not LUMO. However, the narrower E_g could only come from the LUMO drops, with HOMO rising slightly at the same time. Meanwhile, accompanied with different thickness of polymer films, different effective areas of the polymer on ITO, along with the tighter aggregation of P2 and P4 than P1 and P3, the half wave potentials of P1 and P3 are lower than the others. Seen from Fig. 4(a), CV curves of the P2 and P4 exhibit a couple of redox peaks which may be attributed to the lack or absence of electrochemical splitting resulting in stable diradicals. On the contrary, the P1 and P3 exhibit two couples of redox waves which can be explained by that the first oxidative peaks can be attributed to oxidation of one of the N atom in a TPA nucleus and the second step ones are resulted from a dication structure formed from radical recombination [32,33]. Meanwhile, the color of all polymers changes almost from yellowish to dark blue, finally dark red.

The E_{HOMO} and the optical band gap (E_g) are obtained by using E_{onset} and the λ_{onset}, respectively. The detailed data are summarized in Table 3 which experimental results of the highest occupied molecular orbital (HOMO) and the lowest unoccupied molecular orbital (LUMO) energy levels of these polymers are in the range from −4.70 to −5.08 eV, and −1.65 to −2.67 eV respectively. TAA plays an important role in the electronic structure and regulation of the polymers. The difference in the position of the nitrogen atoms still causes a difference in their redox potentials, which in turn leads to a slight different HOMO and LUMO of the polymers. P1 and P4 have close reduction potentials, resulting in the similar HOMO and LUMO while P2 and P3 have large difference HOMO, LUMO due to the large reduction potentials.

To further comprehend the influence of molecular structure on the electronic structures and energy levels of the polymers, the HOMO levels and LUMO levels were calculated by using Gaussian 03W program based on B3LYP/6-31G (d, p) set level, and the data are shown in Table 3. Seen from Fig. 4(b) the electron density distribution of the HOMO is mainly located on diamine moiety meanwhile that of the LUMO is mainly located on oxazine ring [34,35]. The theoretical data of the HOMO and LUMO levels are in the range from −4.65 to −4.91 eV, and −0.97 to −1.05 eV, respectively. The sequence theoretical data of E_g values among the four polymers is P2 < P4 < P1 < P3 which is little different from the experiment results order of the P2 < P1 < P4 < P3. P2 has the least E_g contrast to the P3 with the largest E_g. The little deviation between theory calculation and experiment results from CVs due to the theoretical results are calculated from the repetition unit not from the long chain and the impact interaction of molecules and solvent and aggregation of polymers in solvent are not considered together [36]. Also, electrochemical impedance spectroscopy (EIS) technique can be used to

Table 3

Electrochemical properties and quantum calculations of the polymers.

Polymer code	λ_{onset}^{abs} [a]	E_{onset}^{peak} [b] Ag/AgCl	$E_{HOMO}^{electro}$ [c]	$E_{LUMO}^{electro}$ [c]	E_g [d]	$E_{HOMO}^{quantum}$ [e]	$E_{LUMO}^{quantum}$ [e]	$E_g^{quantum}$ [e]
P1	501	0.52	−4.87	−2.39	2.48	−4.80	−0.98	3.82
P2	514	0.73	−5.08	−2.67	2.41	−4.65	−0.97	3.68
P3	406	0.35	−4.70	−1.65	3.05	−4.91	−0.98	3.93
P4	492	0.53	−4.88	−2.36	2.52	−4.79	−1.05	3.74

[a] λ_{onset} of polymer film.

[b] E_{onset}^{peak}: onset potential of the polymer CV curve was obtained by making a tangent line on cyclic voltammetry.

[c] The HOMO energy levels are calculated from cyclic voltammetry referenced to oxidation potential of ferrocene (4.8 eV).

[d] $E_{HOMO}=-(E_{OX}-E_{\frac{1}{2}(Fc)})$ eV + (−4.8) eV; $E_g^{film}=1240/\lambda_{onset}$; E_{LUMO} (eV) = $E_{HOMO}+E_g^{film}$.

[e] Quantum theoretical calculation of these polymers.

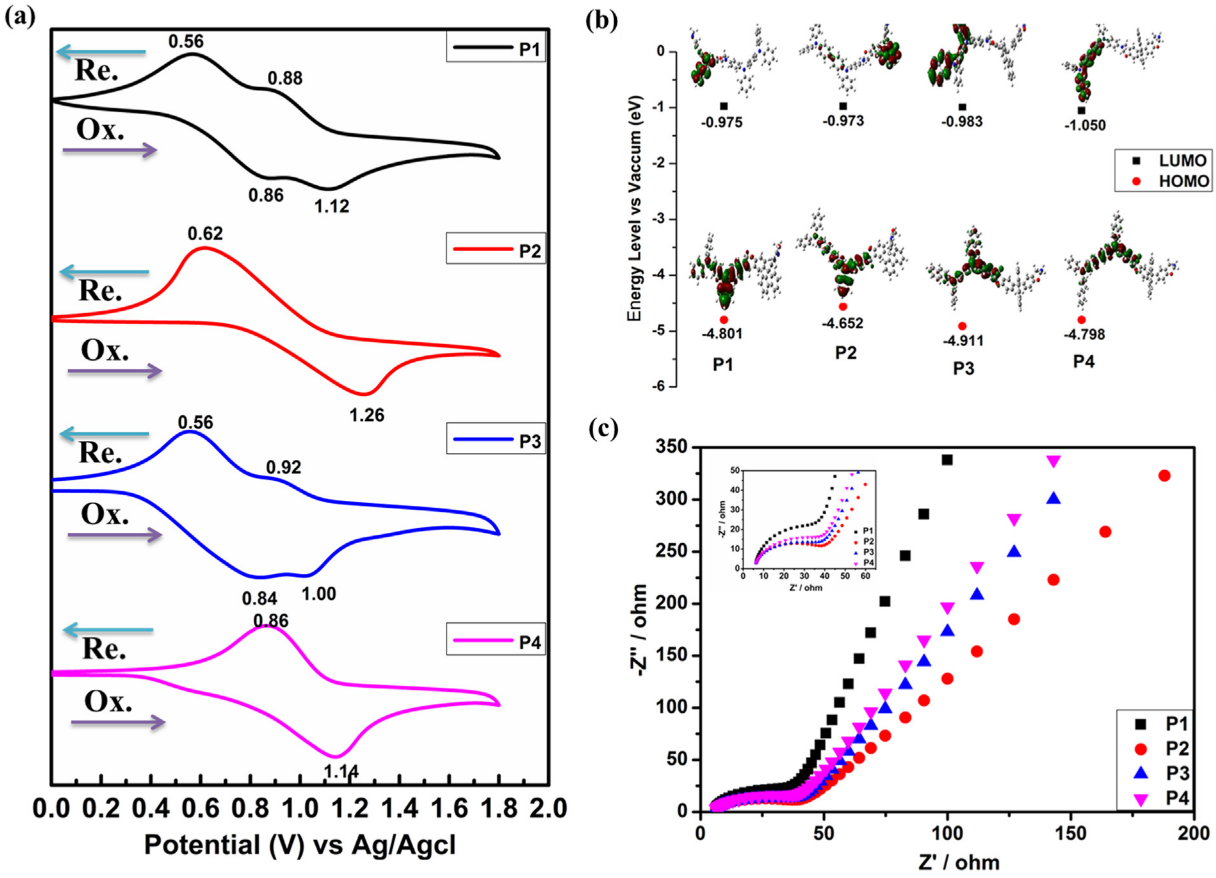

Fig. 4. CV scanning of the polymers on the ITO/glass electrode in 0.2 mol·L^{-1} $LiClO_4/CH_3CN$ solution at a scanning rate of 50 mV·s^{-1} (the arrow indicating the direction of scanning) (a). Graphics of the electron density in the frontier molecular orbitals of repetition units (b). Impendence spectra (c) of P1, P2, P3 and P4.

determine the mechanism of conductivity of ion. The impedance data were fitted by the ZsimDemo software. From Fig. 4(c) the curves can be divided into two parts in which the represents charge transfer resistance of electrons and ions locate at semicircle of high frequency region and the oblique line of low frequency band [37]. The specific impedance data values are summarized in Table S3. R_{ct} is a representative datum for the EC performance. From the Table S3, All the four polymers have relatively low resistance values, and P2 has the largest resistance values compared with the other three polymers, which means P2 has the longer response time.

3.5. EC characteristics

Fig. 5(a) shows a series of EC spectroelechemical curves of polymers upon corresponding applied potentials (from 0.0 to 1.8 V). In the neutral state, there are strong absorption peaks at the wavelengths range between 360 and 390 nm. With the potential applied, new absorptions appear at wavelengths around 440 nm to 700 nm and 900 nm to 1100 nm, respectively. Take P2 for example, there is a characteristic absorption at around 320 nm corresponding to the π–π* transition of TAA moieties. Meanwhile, the color of the polymer film is yellowish in the neutral state with high transmittance as shown in Fig. 5(b). Accompanied with the voltage increasing from 0 to 0.8 V, a new absorbance emerges at 480 nm in Fig. 5(a), while the polymer film color changes from yellowish to dark blue and the transmittance gradually decrease in Fig. 5(b). Until the voltage is increased to 1.8 V, there is obvious absorbance peaks appear at the range of 930 nm, and the color of the polymer film changes dark red. At the same time, the lowest transmittance is reached in Fig. 5(b). However the spectrum does not change obviously because of the TAA having been completely oxidized [38]. The EC absorption of P1, P3 and P4 are shown in Fig. S4, Fig. S5 and Fig. S6, respectively. From Fig. 5(d), the EC mechanism of P2 is explained by that the TPA from neutral state in yellowish turns to intermediate state in blue and finally changes to oxidized state in dark red which could be attributed to the electronic transfer of TAA → TAA^{2+}.

In order to further investigate the stability of the polymer EC films, it is necessary to obtain the transmittance change (Δ%T) and the response time which are measured by repeating step potential during the polymer films change from neutral to oxidized state [39]. The EC materials are used as the smart windows with fast response time, good film stability and the color efficiency (CE). In this study the polymer films exhibit better EC reversibility after 500 s of being reduced and oxidized at the given wavelength. It indicates that the polymer films are very stable and the adhesion force to the ITO substrate is very strong. Take P2 as an example, in the Fig. 5(e), when the wavelength is set at 930 nm with applied voltage of 1.4 V the coloring and the bleaching time are 2.3 s and 2.0 s, respectively. The results are collected in Table S2 and the transmittance spectra are provided in Fig. S7(a), (b), and (c).

3.6. ECD characteristics

To improve the contrast of the device before and after oxidation and evaluate the application of the polymers, a solid-state device was assembled by the active polymer film coated on ITO working as the anode, tungsten trioxide (WO_3) coated on ITO working as the cathode,

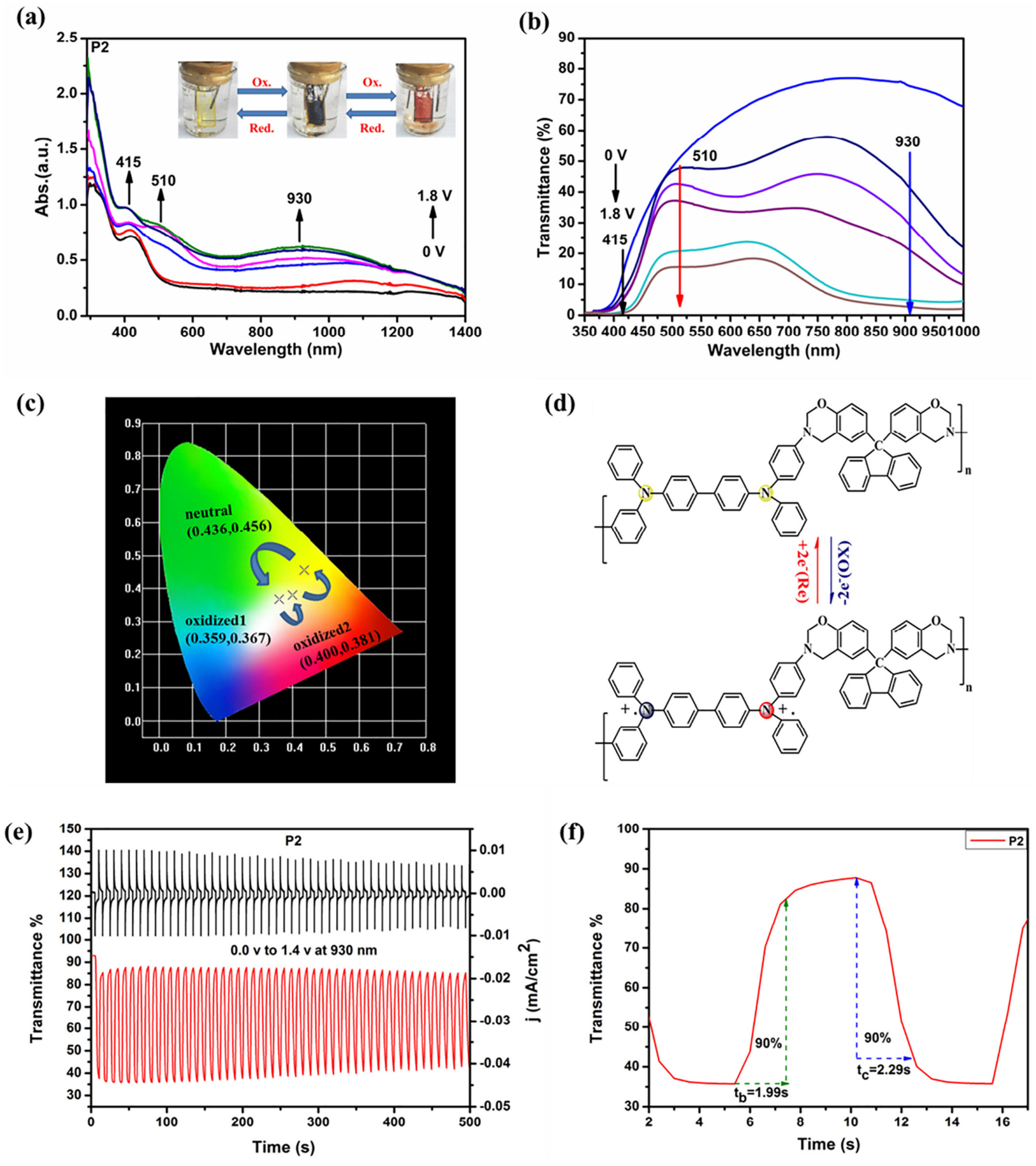

Fig. 5. Electronic absorption spectra (a) transmittance spectra (b) and the color coordinate (c) proposed EC mechanism (d) dynamic changes of the transmittance and current (e); optical switching (f) of P2 film in $LiClO_4$/CH_3CN solution upon application of different voltages. (For interpretation of the references to color in this figure, the reader is referred to the web version of this article.)

lithium perchlorate ($LiClO_4$) in mixture of polymethyl methacrylate (PMMA) and propylene carbonate (PC) solution working as gel electrolyte with polyethylene terephthalate (PET) as spacer, respectively. The solid-state device is easier to be assembled than the device with liquid electrolyte, as well as the performance is more stable. Finally, the device is sealed by epoxy resin. The schematic of device and photos of electrochromic performance are shown in Fig. 6(a). The simple device exhibits a more pronounced color change when the voltage was

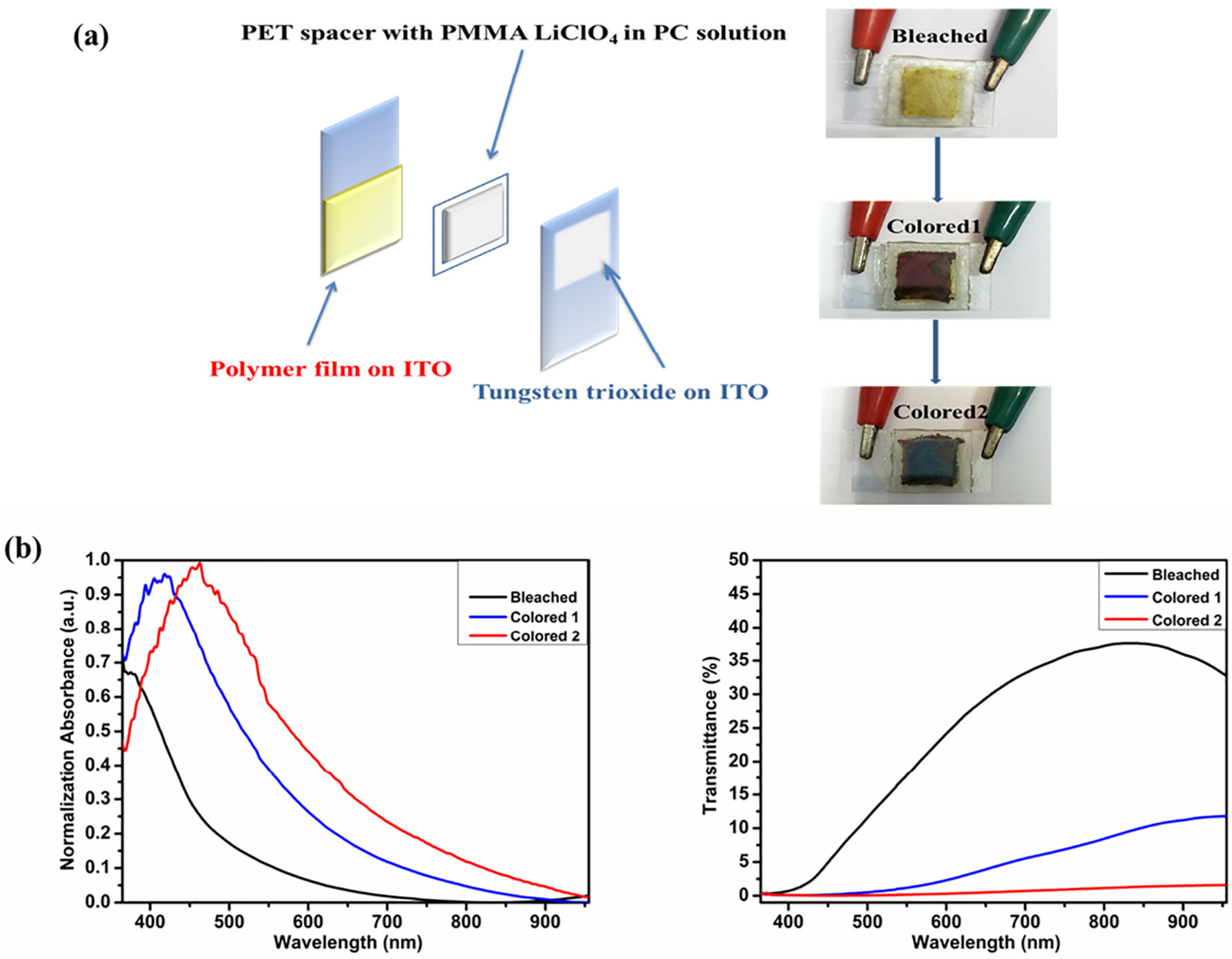

Fig. 6. Schematic of EC device with P2 electrode and pictures of color changing of device (a). UV–vis spectra (b) and change in transmittance (b) for solid-state ECD upon application of an external voltage. (For interpretation of the references to color in this figure, the reader is referred to the web version of this article.)

increased from 0 to 0.6 V. The color of device changed from the initial film light yellow to dark purple, and finally to the dark blue with three color states. A simple optical characteristics test was carried out on the solid-state device through an electrochemical workstation, and it can be seen from the Fig. 6(b) that the UV–visible absorption of the solid-state device shows noticeable change when different states are displayed. In the meantime, the transmittance of the device is shown in Fig. 6(c), and it is worth noting that the transmittance is nearly 50 in bleached state and is lowest in colored state of the ECD. Compared with liquid electrolyte and single electrode of previous work [40], the performances of this solid-state device before and after being applied voltage are more excellent, and the color contrast of the device is more obvious.

3.7. Explosives detection

TNT and TNP are the dangerous explosives which are damage to security, environment [41], and health (including lung damage, and skin irritation for human beings). So, to investigate the detection properties of TNT and TNP sensors, the PL quenching experiments was carried out to detect explosives by adding the TNT/TNP into the solutions of these polymers. Take P2 for example, the emission maximum of P2 in NMP appears at 475 nm. As the concentration of TNT gradually increases, the PL intensity of polymer solution decreases. In Fig. 7(a) and (b), all the PL intensities of polymer solution show a similar downward tendency which indicate that P2 can respond to TNT and TNP selectively. Compared to P2 and P4, the PL intensities of P1 and P3 are weak. Therefore, here P1 and P3 are not the first choice for detecting explosives. The performance of P4 is shown in Fig. S8(a) and (b). Fig. 7(c) and (d) reveals the linear relationship of TNT or TNP concentration to quenching rate ($I_0/I-1$). And the inset exhibits the linear fit at the concentration range from 0 μM to 40 μM of TNT or TNP. The mechanism of quenching is understood by that TNT and TNP are strong electron acceptors, when PBZ is arriving to TNT or TNP, electrons flow from the donor to the acceptor. Meanwhile, Stern-Volmer quenching constant (K_{SV}) can be obtained by formula (3) [42]. Take P2 as an example, according to formula, K_{SV}s of TNP and TNT are calculated to be 33,370 M^{-1} and 51,360 M^{-1}, respectively. One can conclude that P2 has higher sensitivity to TNT than others.

$$\frac{I_0}{I}=1+K_{SV}[Q] \tag{3}$$

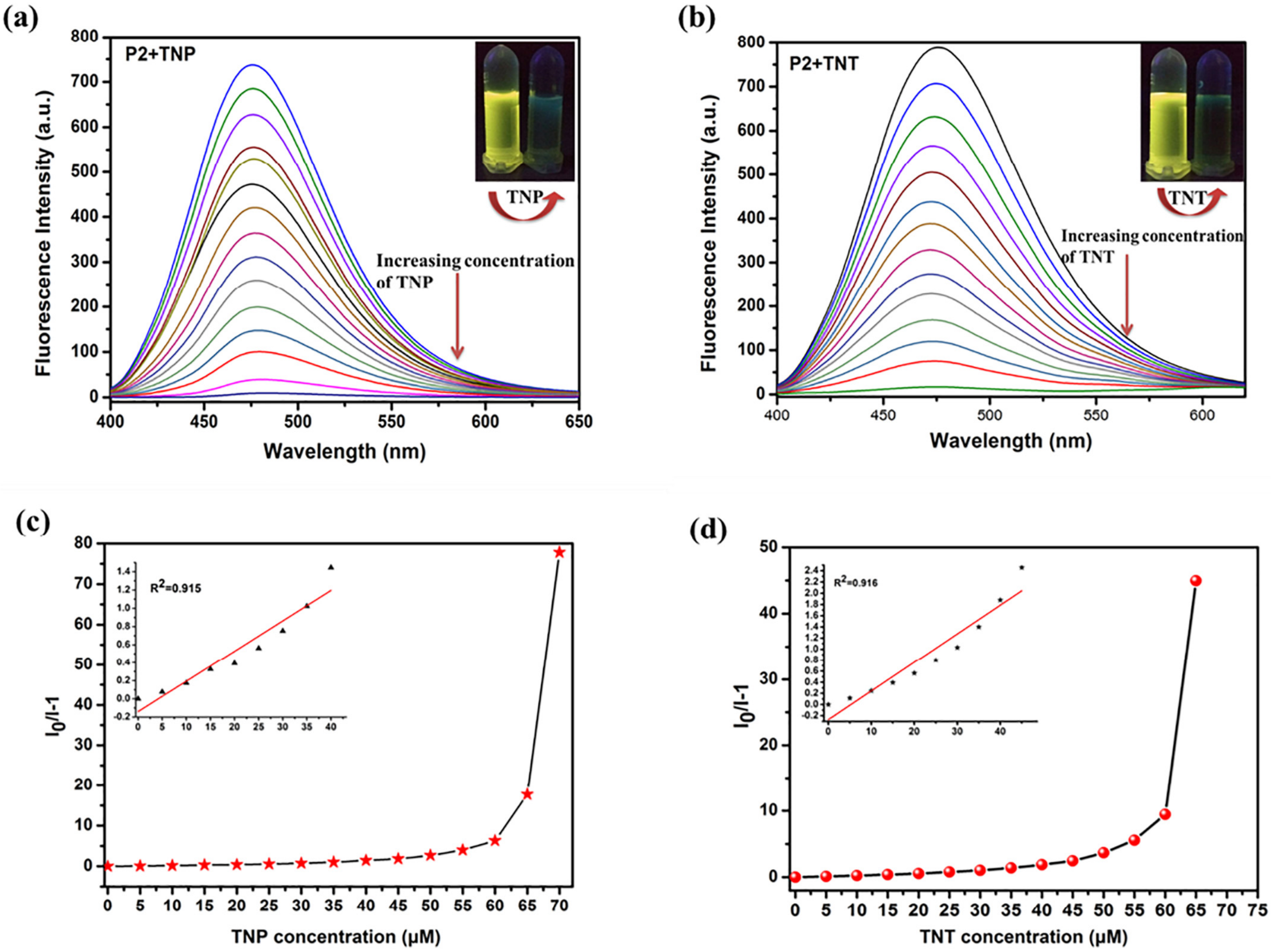

Fig. 7. Changes in PL spectra of P2 (5 μg/mL) under regularly TNP (0–75 μg/mL) (a); TNT (0–60 μg/mL) (b) added. The dependence of PL intensities upon TNT (c) and TNP (d) concentration (inset: calibration curves of K_{sv}. I and I_0 are PL intensities with or without polymer solution respectively).

3.8. Resistance memory performance

These resistance memory devices are made up by a simple sandwich-shaped structure in which the polymer film works as an active layer, Al works as top electrode and ITO works as the bottom electrode, respectively. Illustration of the resistance memory device is depicted in Fig. 8(a). The electrical conductance memory performances of device is showed through the current–voltage (I-V) characteristics curves in Fig. 8(b). All the polymers show similar memory behaviors, P3 is chosen as an example. As shown in Fig. 8(b), a typical I-V characteristic curve is constituted by four steps scan with the different applied voltage. The process is called as "write-read-erase-reread" (WRER) with the increase of the applied voltage [43]. Firstly, the conduction process of the "writing" describes that the resistance memory device with the sweep comes up a sharp at −2.2 V from high resistance state (HRS) to low resistance state (LRS) [44]. Then, during the second sweep, the device remains LRS state which is defined "reading" step in a digital memory. In the third scan during the reverse bias from 0 to 6 V, it is in HRS state. However, the current suddenly goes downward and back to the original low conductive state at near 4.0 V which is called "erasing". The fourth sweep remains "OFF" state during 0 to −8 V. I-V characteristics of P1, P2 and P4 are shown in Fig. S9(a), (b) and (c), respectively. Memory mechanism in the view of energy level is analyzed. From the Fig. 8(c), the electron is injected from Al electrode to the LUMO and the hole is injected from ITO electrode to the HOMO of the P3, in which the energy barriers are 3.29 eV and 0.11 eV, respectively. It can be concluded that the memory device conduction process is dominated by the hole injection energy barrier other than by the electron injection due to the hole barrier is too high to prevent the migration of electrons. At the negative voltage (0 to −2.2 V), the holes are gently injected from ITO electrode into the HOMO energy of the P3. When the scan voltage is increased to the threshold voltage, sufficient energy is supplied to the electrons on the Al electrode to surmount the energy barrier between Al and LUMO for injection into the active layer. At the moment, when the voltage is further increased, since the holes and electrons have sufficiently high mobility, a conductive road is formed from the Al electrode to the ITO electrode, and the current passes through the road and the device maintains the in an ON state.

4. Conclusions

In this study, a series of new TAA-based with main-chain BZ polymers were successfully facilely synthesized by Mannich reaction with the diamines. The four polymers showed a good behavior in EC, resistance memory performance and explosive detection. In EC behavior, the polymer films showed obvious color changes that from yellowish

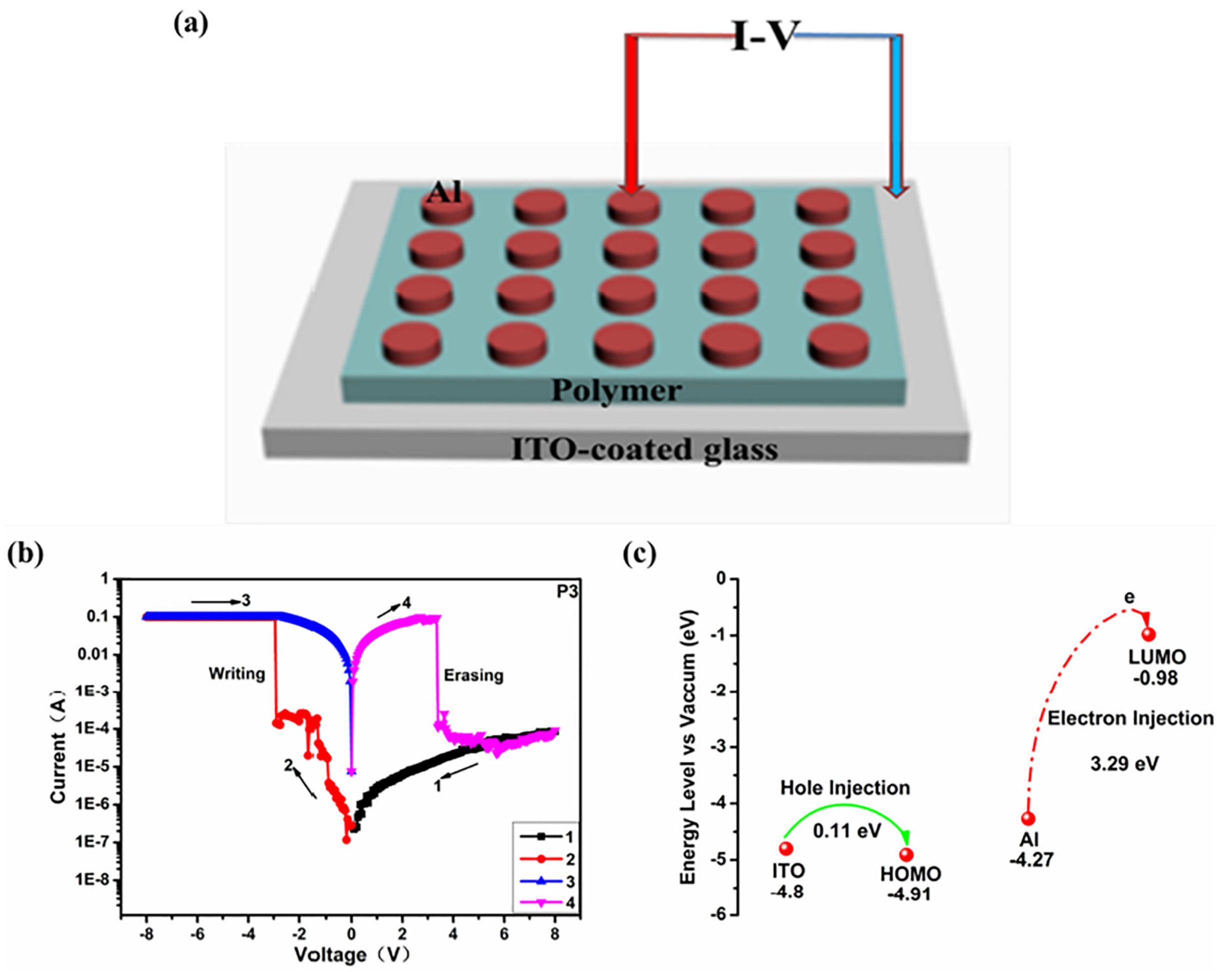

Fig. 8. (a) Schematic of the memory device; (b) I-V curves of P3 and (c) energy level diagram of the ITO/P3/Al memory device.

in neutral state to dark red in final oxidized state with the voltage being applied and the films could remain the excellent stability. Moreover, these polymers could not only achieve explosive detection through PL quenching mechanism, but also could be applied in digital memory devices. In summary, the polymers will be promising candidates for optoelectronic field.

Acknowledgements

This work was supported by the National Natural Science Foundation of China (51773053); Heilongjiang Province Foundation for Returners from Oversea (LC2018024); Heilongjiang University Graduate Innovation Fund (YJSCX2019-078HLJU). Innovation and entrepreneurship program for college students (201910212039).

Declaration of competing interest

The authors declare no conflict of interest.

Appendix A. Supplementary data

Supplementary data to this article can be found online at https://doi.org/10.1016/j.saa.2019.117524.

References

[1] R. Ponnapati, M.J. Felipe, V. Muthalagu, K. Puno, B. Wolff, R. Advincula, Conjugated polymer network films of poly(p-phenylene vinylene) with hole-transporting carbazole pendants: dual photoluminescence and electrochromic behavior, ACS Appl. Mater. Interfaces 4 (2012) 1211–1218.

[2] N.E. Dov, S. Shankar, D. Cohen, T. Bendikov, K. Rechav, M. Lahav, M.E. Boom, Electrochromic metallo-organic nanoscale films: fabrication, color range, and devices, J. Am. Chem. Soc. 139 (2017) 11471–11481.

[3] R.Z. Zheng, J.Q. Zhang, C.Y. Jia, Z.Q. Wan, Y.R. Fan, X.L. Weng, J.L. Xie, L.J. Deng, A novel self-healing electrochromic film based on a triphenylamine cross-linked polymer, Polym. Chem. 8 (2017) 6981–6988.

[4] S.-H. Hsiao, J.-Y. Lin, Electrosynthesis of ambipolar electrochromic polymer films from anthraquinone-triarylamine hybrids, J. Polym. Sci. Part A: Polym. Chem. 54 (2016) 644–655.

[5] W.S. Li, J.Y. Ning, M.W. Qi, Y.W. He, H. Meng, Thieno [3,2-b]thiophene-based conjugated copolymers for solution-processable neutral black electrochromism, Polym. Chem. 9 (2018) 5608–5616.

[6] G.F. Cai, J.X. Wang, P.S. Lee, Next-generation multifunctional electrochromic devices, Acc. Chem. Res. 49 (2016) 1469–1476.

[7] C. Mallet, M.L. Borgne, M. Starck, W.G. Skene, Unparalleled fluorescence of a polyazomethine prepared from the self-condensation of an automer and its potential use as a fluorimetric sensor for explosive detection, Polym. Chem. 4 (2013) 250–254.

[8] B. Berns, B. Tieke, Electrochromic polyiminocarbazolylenes with latent hydrogen bonding, Polym. Chem. 6 (2015) 4887–4901.

[9] W.J. Zhang, C.R. Zhu, Z.J. Huang, C.B. Gong, Q. Tang, X.K. Fu, Electrochromic 2,4,6-triphenyl-1,3,5-triazine based esters with electron donor-accept structure, Org. Electron. 67 (2019) 302–310.

[10] C. Ma, M. Taya, C.Y. Xu, Smart sunglasses based on electrochromic polymers, Polym. Eng. Sci. 48 (2008) 2224–2228.

[11] S. Beaupre, A.-C. Breton, J. Dumas, M. Leclerc, Multicolored electrochromic cells based on poly(2,7-carbazole) derivatives for adaptive camouflage, Chem. Mater. 21 (2009) 1504–1513.

[12] S. Shao, J.J. Shi, I. Murtaza, P.P. Xu, Y.W. He, S. Ghosh, X.S. Zhu, I.F. Perepichka, H. Meng, Exploring the electrochromic properties of poly(thieno[3,2-b]thiophene)s decorated with electron-deficient side groups, Polym. Chem. 8 (2017) 769–784.

[13] J.C. Wu, Y.F. Han, J. Liu, Y.C. Shi, J.M. Zheng, C.Y. Xu, Electrofluorochromic and electrochromic bifunctional polymers with dual-state emission via introducing multiple C-H… π bonds, Org. Electron. 62 (2018) 481–490.

[14] D. Weng, M. Li, J.M. Zheng, C.Y. Xu, High-performance complementary electrochromic device based on surface-confined tungsten oxide and solution-phase N-methyl-phenothiazine with full spectrum absorption, J. Mater. Sci. 52 (2017) 86–95.

[15] C.X. Li, C.L. Liu, L. Shi, G.M. Nie, Electrochemical copolymerization of 3,4-ethylenedioxythiophene and 6-cyanoindole and its electrochromic property, J. Mater. Sci. 50 (2015) 1836–1847.

[16] W.A. Cai, Q.Y. Lu, S.Z. Wang, T.D. Xiao, H.J. Niu, W. Wang, Synthesis and characterization of stable electrochromic polyimides with quinolin-8-yloxy-substituted triphenylamine units, J. Electroanal. Chem. 801 (2017) 388–394.

[17] U. Thubsuang, S. Wongkasemjit, H. Ishida, T. Chaisuwan, Improvement in the pore structure of polybenzoxazine-based carbon xerogels through a silica templating method, J. Porous. Mater. 21 (2014) 401–411.

[18] N.N. Gosh, B. Kiskan, Y. Yagci, Polybenzoxazines—new high performance thermosetting resins: synthesis and properties, Prog. Polym. Sci. 32 (2007) 1344–1391.

[19] X. Ning, H. Ishida, Phenolic materials via ring-opening polymerization: synthesis and characterization of bisphenol-A based benzoxazines and their polymers, J. Polym. Sci. Part A: Polym. Chem. 32 (1994) 1121–1129.

[20] C.H. Lin, S.L. Chang, C.W. Hsieh, H.H. Lee, Aromatic diamine-based benzoxazines and their high performance thermosets, Polymer 49 (2008) 1220–1229.

[21] C.H. Lin, S.L. Chang, T.Y. Shen, Y.S. Shih, H.T. Lin, C.F. Wang, Flexible polybenzoxazine thermosets with high glass transition temperatures and low surface free energies, Polym. Chem. 3 (2012) 935–945.

[22] C.R. Arza, P. Froimowicz, L. Han, R. Graf, H. Ishida, Design, synthesis, characterization, and polymerization of fused-ring naphthoxazine resins, Macromolecules 50 (2017) 9249–9256.

[23] M.G. Mohamed, S.W. Kuo, Functional silica and carbon nanocomposities based on polybenzoxazines, Chem. Phys. 220 (2018) 1800306–1800319.

[24] J.W. Cai, L.N. Ma, H.J. Niu, P. Zhao, Y.F. Lian, W. Wang, Near infrared electrochromic naphthalene-based polyimides containing triarylamine: synthesis and electrochemical properties, Electrochim. Acta 112 (2013) 59–67.

[25] H.J. Niu, J.W. Cai, P. Zhao, C. Wang, X.D. Bai, W. Wang, Simple approach to regulate the spectra of novel kinds of polyazomethines containing bulky triphenylamine: electrochemistry, electrochromism and photophysical responsive to environment, Dyes Pigments 96 (2013) 158–169.

[26] J. Bae, H. Kim, H.C. Moon, S.H. Kim, Low-voltage, simple WO_3-based electrochromic devices by directly incorporating an anodic species into the electrolyte, J. Mater. Chem. C 4 (2016) 10887–10892.

[27] K.L. Zhou, H. Wang, S.J. Zhang, J.T. Jiu, J.B. Liu, Y.Z. Zhang, H. Yan, Electrochromic modulation of near-infrared light by WO_3 films deposited on silver nanowire substrates, J. Mater. Sci. 52 (2017) 12783–12794.

[28] W.H. Chen, K.L. Wang, W.Y. Hung, J.H. Jiang, D.J. Liaw, K.R. Lee, J.Y. Lai, C.L. Chen, Novel triarylamine-based alternating conjugated polymer with high hole mobility: synthesis, electro-optical, and electronic properties, J. Polym. Sci. Part A: Polym. Chem. 48 (2010) 4654–4667.

[29] H.-M. Wang, S.-H. Hsiao, Ambipolar, multi-electrochromic polypyromellitimides and polynaphthaalimides containing di(tert-butyl)-substituted bis(triarylamine) units, J. Mater. Chem. C 2 (2014) 1553–1564.

[30] C.X. Xu, J.S. Zhao, J.S. Yu, C.S. Cui, Ethylenedioxythiophene derivatized polynapthalenes as active materials for electrochromic devices, Electrochim. Acta 96 (2013) 82–89.

[31] X.F. Cheng, J.S. Zhao, C.S. Cui, Y.Z. Fu, X.X. Zhang, Star-shaped conjugated systems derived from thienyl-derivatized poly(triphenylamine)s as active materials for electrochromic devices, J. Electroanal. Chem. 677-680 (2012) 24–30.

[32] X.C. Ma, H.J. Niu, H.L. Wen, S.H. Wang, Y.F. Lian, X.D. Bai, W. Wang, Synthesis, electrochromic, halochromic and electro-optical properties of polyazomethines with a carbazole core and triarylamine units serving as functional groups, J. Mater. Chem. C 3 (2015) 3482–3493.

[33] X.T. Wu, W. Wang, B. Li, Y.J. Hou, H.J. Niu, Y.H. Zhang, S.H. Wang, X.D. Bai, Synthesis and electrochromic, acidochromic properties of Schiff based containing triphenylamine and thiophene units, Spectrochim. Acta A Mol. Biomol. Spectrosc. 140 (2015) 398–406.

[34] Q.Y. Lu, W.A. Cai, H.J. Niu, W. Wang, X.D. Bai, Y.J. Hou, Novel polyamides with 5H-dibenzo[b,f] azepin-5-yl-substituted triphenylamine: synthesis and visible-NIR electrochromic properties, Polymers 10 (2017) 542–564.

[35] T.C. Chu, X.P. Ju, X. Han, H.M. Du, Y. Zhang, J.S. Zhao, J.H. Zhang, Synthesis and electrochromic properties of cross-linked and soluble conjugated polymers based on 5,8,14,17-tetrabromoquinoxaline [2′,3′:9,19] phenanthro [4,5-abc] phenazine as the multifunctionalized acceptor unit, Org. Electron. 73 (2019) 43–54.

[36] L.-C. Lin, H.-J. Yen, Y.-R. Kung, C.-M. Leu, T.-M. Lee, G.-S. Liou, Novel near-infrared and multi-colored electrochromic polybenzoxazines with electroactive triarylamine moieties, J. Mater. Chem. C 2 (2014) 7796–7803.

[37] X.C. Sun, J.K. He, Y.T. Meng, L.C. Zhang, S.C. Zhang, X.Y. Ma, J. Zhao, Microwave-assisted ultrafast and facile synthesis of fluorescent carbon nanoparticles from a single precursor: preparation, characterization and their application for the highly selective detection of explosive picric acid, J. Mater. Chem. A 4 (2016) 4161–4171.

[38] X.L. Liu, L.Q. Kong, H.M. Du, Y. Zhang, J.S. Zhao, Y. Xie, Synthesis and electrochromic properties of electrochromic polymers based on propylenedioxythiophene, diketopyrrolopyrrole and benzodithiophene units, Org. Electron. 64 (2019) 223–235.

[39] Y. Zhou, X.C. Liu, X.T. Jia, D.M. Chao, Synthesis and electrochromic properties of a graphene oxide/silicon dioxide/oligoaniline interpenetrating network composite, New J. Chem. 43 (2019) 3829–3834.

[40] Q.Y. Lu, X. Zhang, W.A. Cai, Y. Wang, C.Y. Yang, Y. Chen, Donor-acceptor conjugated polymers containing isoindigo block for novel multifunctional materials for electrochromic, resistance memory, and detector devices, Sol. Energy Mater. Sol. Cells 200 (2019) 109979–109990.

[41] C. Muthu, S.R. Nagamma, V.C. Nair, Luminescent hybrid perovskite nanoparticles as a new platform for selective detection of 2,4,6-trinitrophenol, RSC Adv. 4 (2014) 55908–55911.

[42] Z.M. Gou, Y.J. Zuo, M.G. Tian, W.Y. Lin, Siloxane-based nanoporous polymers with narrow pore-size distribution for cell imaging and explosive detection, ACS Appl. Mater. Interfaces 10 (2018) 28979–28991.

[43] M.-C. Tsai, C.-L. Wang, C.-Y. Lin, C.-L. Tsai, H.-J. Yen, H.-C. You, G.-S. Liou, A novel porphyrin-containing polyimide for memory devices, Polym. Chem. 7 (2016) 2780–2784.

[44] Y.Q. Li, M.Y. Zhou, Z.W. Yang, Y. Li, Anthraquinone-functionalized polyurethane designed for polymer electrochromic and electrical memory applications, J. Mater. Sci. 53 (2018) 15600–15613.